J Mater Sci (2007) 42:6188–6196
DOI 10.1007/s10853-006-1165-6

Physico-chemical study of impregnated Cu and V species on CeO_2 support by thermal analysis, XRD, EPR, ^{51}V-MAS-NMR and XPS

Renaud Cousin · Edmond Abi-Aad · Sylvie Capelle · Dominique Courcot · Jean-François Lamonier · Antoine Aboukaïs

Received: 20 September 2005 / Accepted: 19 October 2006 / Published online: 20 April 2007

Abstract CuVCe oxides were prepared by impregnation of copper and/or vanadium precursors on ceria support. The solids freshly prepared were calcined under air between 400 and 700 °C. Physico-chemical properties of these oxides were then studied using different techniques: Thermal Analysis (DSC/TG), X Ray Diffraction (XRD), Electron Paramagnetic Resonance (EPR), ^{51}V Magic Angle Spinning Nuclear Magnetic Resonance (^{51}V-MAS-NMR) and X-Ray Photoelectron Spectroscopy (XPS). X-ray diffraction and thermal analysis revealed cerium orthovanadate phase formation during the calcination of the 1Cu1V10Ce solid. This $CeVO_4$ phase is not observed for the 10Cu1V10Ce sample. The EPR study revealed two well-resolved copper signals: the first corresponds to isolated Cu^{2+} species and the second to Cu^{2+} dimers. The ^{51}V-MAS-NMR confirmed the presence of $CeVO_4$ phase for 1Cu1V10Ce sample and revealed polymeric V–O–V chains in interaction with a copper ceria matrix for 10Cu1V10Ce sample. Finally, the XPS study indicated high vanadium content on the solid surface. This phenomenon is enhanced by the copper content in the solid and could explain the absence of the $CeVO_4$ phase in 10Cu1V10Ce sample. Thus the ceria orthovanadate phase formation is inhibited by the presence of a high copper content in the solid.

R. Cousin (✉) · E. Abi-Aad · S. Capelle · D. Courcot · J.-F. Lamonier · A. Aboukaïs
Laboratoire de Catalyse et Environnement, E.A. 2598, Université du Littoral Côte d'Opale, 145 avenue Maurice Schumann, 59140 Dunkerque, France
e-mail: Renaud.Cousin@univ-littoral.fr

Introduction

In recent years, the oxides such as CeO_2, V_2O_5 and CuO have received considerable attention for oxidation catalysis. These systems can lead to interesting catalytic properties in the depollution reactions [1–5]. CeO_2 is well known for its low temperature reducibility, oxygen storage and release properties in the presence of noble metal particles. The redox couple (Ce^{3+}/Ce^{4+}) in contact with metal particles promotes the catalytic activity in ceria-based materials [6–10].

Cu-modified fluorite-CeO_2 compounds have been reported to be active catalysts for many reactions. The conventional co-precipitation and impregnation methods are widely employed to prepare CuO/CeO_2 materials [2, 4, 11–14] in which the interaction of CuO with fluorite-CeO_2 has been studied by thermal, surface and bulk techniques. These studies generally show the existence of (i) amorphously dispersed active surface Cu^{2+} clusters, (ii) small crystallites of CuO dispersed on CeO_2 particles, (iii) isolated Cu^{2+} ions and Cu^{2+} dimers incorporated in ceria and (iv) Cu^{2+} ions in substitutional positions in the ceria lattice depending on the preparation procedure, composition and thermal treatment. It has also been reported that during preparation, some CuO may enter into CeO_2 lattice forming solid solutions which act as support for Cu^{2+} clusters and small CuO particles [2].

Vanadia supported on various oxide carriers is used as catalyst in different oxidation processes [15–18]. It has been also proved to be quite effective for the selective catalytic reduction (SCR) of nitric oxide. It has been demonstrated that the selectivity and activity of these catalysts depend on, among other factors, the vanadium loading, calcination temperature, type of support, and its surface acidity. In addition, depending on the nature of the

oxide carrier (i.e. Al_2O_3, TiO_2, MgO, ZrO_2), vanadia oxides may exhibit different catalytic properties, since the metal oxide–support interaction affects both dispersion and redox behaviour of the active phase and also work function properties. However, surface vanadium oxide stability can be limited if ternary compounds of the type $M_xV_yO_z$ are formed between the carrier and the vanadia phase. Indeed, in a previous work [19], we have observed that V_2O_5 can react with CeO_2 carrier at high temperature (≥600 °C) to form the cerium orthovanadate $CeVO_4$ compound. Thus, it provided deep modifications of the supported vanadium phase. Such studies could be provided by the determination of the local structure of these species following the calcinations treatment and the vanadium content. Solid-state ^{51}V-NMR has also been used by various investigators [20–22], toward the determination of the molecular structure of these surface metal oxide species on oxide support due to the favourable magnetic properties of the ^{51}V nucleus. In addition, magic angle spinning experiments (MAS-NMR) provided precise discrimination between different species that may simultaneously be present in the sample.

In order to combine the physicochemical and catalytic properties of these elements (Cu, V and Ce), different oxides constituted by cerium, vanadium and copper have been synthesised. An investigation of the nature of Cu–V–Ce species could provide useful information to understand elementary step in the catalytic reaction. Thus, the objective of this work is to identify the species in Cu–V–Ce oxides and evaluate their stability depending on the copper content.

Experimental

Oxides preparation

Ceria [CeO_2] was prepared by precipitation of cerium hydroxide from cerium nitrate [$Ce(NO_3)_3{\cdot}6H_2O$] with a sodium hydroxide [NaOH] solution as described in reference [23]. The solid was calcined at 700 °C for 4 h under a flow of dried air. Subsequently, vanadyl oxalate [VOC_2O_4] and copper nitrate [$Cu(NO_3)_2{\cdot}3H_2O$] were impregnated on ceria to prepare *x*Cu1V10Ce samples with different atomic content (nearly $x = 0$, 1, or 10). After drying at 100 °C, the solids freshly prepared were calcined between 400 and 700 °C under a flow of dry air for 4 h. Chemical analyses of the different samples give the Cu, V and Ce expected atomic content.

Samples characterization

Thermal Analysis measurements were performed on a Netzsch STA 409 Apparatus. For each dried solid, a mass of 50 mg was considered and placed in an Al_2O_3 crucible. Simultaneous thermo gravimetric-differential scanning calorimetric (TG-DSC) curves were obtained while samples were heated from 50 to 700 °C with a rate of 5 °C min^{-1} under a flow of air.

XRD analysis was performed on a BRUKER Advance D8 powder X-Ray diffractometer using Cu K_α radiation ($\lambda = 0.15406$ nm). The XRD patterns were recorded over a 2θ range of 15–65° and using a step size of 0.02° and step time of 4 s.

The electron paramagnetic resonance (EPR) measurements were performed at –196 °C on a EMX Bruker Spectrometer, using a cavity operating with a frequency of 9.5 GHz (X-Band). The magnetic field was modulated at 100 kHz. The *g* values were determined from precise frequency and magnetic field values.

Magic angle spinning (MAS) ^{51}V-NMR spectra were recorded at room temperature on a Brucker ASX 400 spectrometer operating at 105.2 MHz and equipped with a MAS probe for 4 mm outer diameter rotors. Rotation frequencies of 10–15 kHz have been used. In all experiments, a single pulsed excitation of 1.5 μs was applied, a dead time of 10 μs and a recycle time of 5 s were used. The isotropic chemical shifts were referred to external $VOCl_3$.

XPS spectra were acquired with a VG Escalab spectrometer equipped with a 150 W Al K_α ($hv = 1486.6$ eV) X-ray source. The samples were crushed into a fine powder and pressed onto an indium support, itself fixed to a stainless steel plate. The spectra were recorded under a vacuum of 10^{-8} Torr. The binding energies (E_b) values were determined by using the Ce 3d satellite peak at 916.7 eV for standardisation.

Results and discussion

Thermal analysis

The TG-DSC curves of 1V10Ce, 1Cu1V10Ce and 10Cu1V10Ce are illustrated in Fig. 1. Characteristics of these thermal data, i.e., mass loss and temperature of thermal phenomenon, are presented in Table 1. For 1V10Ce solid, a weight loss of 1.65% associated with a broad endothermic phenomenon was evidenced at low temperature (<160 °C) and corresponds to the removal of water. The second weight loss of 3.75% between 160 and 300 °C was associated with an intense exothermic peak that could indicate the oxidation of the organic function of the VOC_2O_4 precursor. This exothermic peak was assigned to the oxalate decomposition [24]. Finally, a slight weight loss of 0.14% obtained between 450 and 700 °C was ascribed to the formation of $CeVO_4$ from vanadium (V) oxide and ceria, and this is in agreement with our previous work on V–Ce–O catalysts using EPR and ^{51}V-MAS-NMR

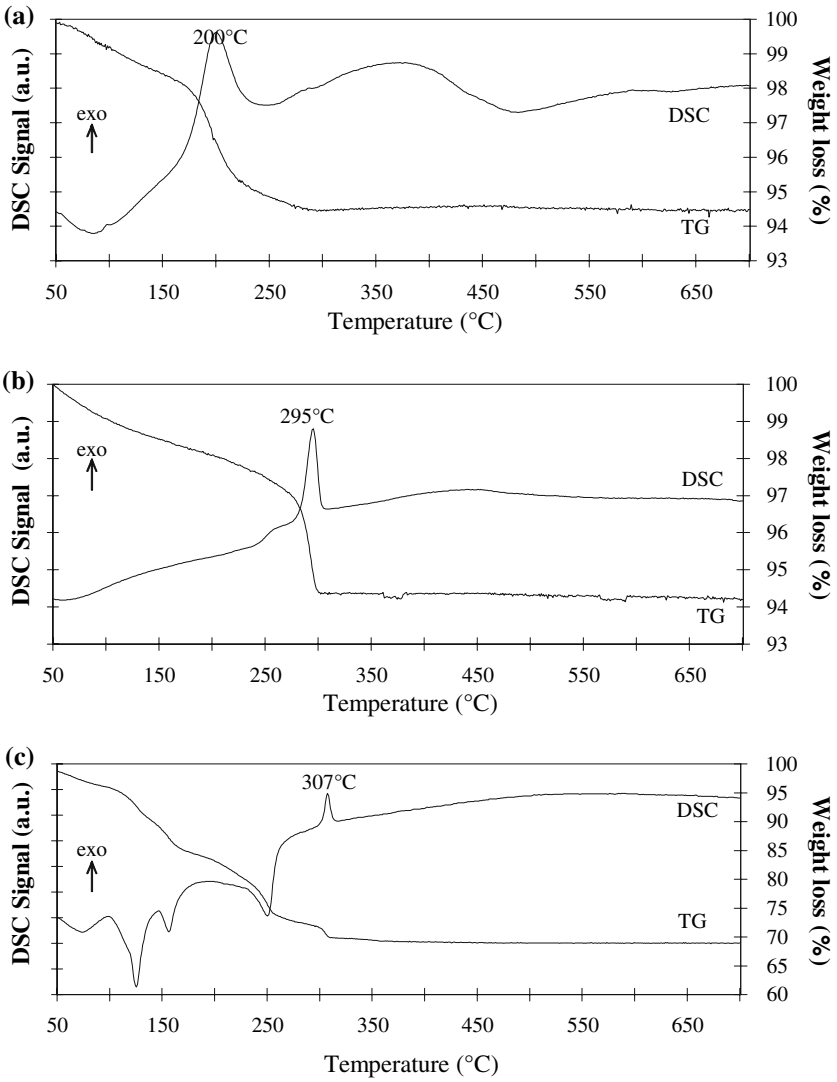

Fig. 1 TG-DSC curves of 1V10Ce (**a**), 1Cu1V10Ce (**b**) and 10Cu1V10Ce (**c**) dried samples

Table 1 Thermogravimetric data of solids and their attribution

Sample	Experimental data		Attribution	
	Temperature (°C)	Weight loss (%)	Transformation	Calculated weight loss (%)
1V10Ce	50–160	1.65	Water removal	–
	160–300	3.75	Decomposition of oxalate	3.41
	450–700	0.14	Partial formation of $CeVO_4$	0.44
1Cu1V10Ce	50–305	5.90	Water removal and decomposition of precursors	–
	450–700	0.16	Partial formation of $CeVO_4$	0.39
10Cu1V10Ce	50–350	30.93	Water removal and decomposition of precursors	–
	450–700	–	Nothing	–

[19, 25]. Concerning the 1Cu1V10Ce sample, similar phenomena could be observed. At low temperature, (<305 °C) endothermic and exothermic peaks associated with weight loss correspond to water removal and progressive decomposition of precursor (oxalate and nitrate). We could also observe a slight weight loss between 450 and 700 °C corresponding to the $CeVO_4$ formation phase. However, the thermal analysis of the 10Cu1V10Ce sample presented a characteristic water removal and precursor decomposition at low temperature (<350 °C), but no weight loss at a temperature range of 450–700 °C is observed. It seems that no $CeVO_4$ phase is formed for the

10Cu1V10Ce solid. In order to investigate the influence of the copper content on the $CeVO_4$ phase in the Cu–V–Ce oxide, the XRD analyses were performed to evaluate the different phases or solid structure.

X-ray diffraction

Figure 2 shows the XRD patterns obtained for the different solids previously calcined at 400, 500, 600 and 700 °C. A ceria phase is evidenced in all the solids. This phase is typical from cerianite structure (JCPDS-ICDD: 43-1002). For 1V10Ce solid, a $CeVO_4$ phase is revealed (JCPDS-ICDD: 12-757) when the solid is calcined up to 500 °C. This formation phase was already studied in previous works [18, 19, 25, 26]. It was shown by EPR and XRD techniques that the formation of $CeVO_4$ phase from CeO_2 and V_2O_5 occurs via an intermediate step in which an electron is trapped in non-stoichiometric oxides like V_2O_{5-x} and CeO_{2-y} matrices which are obtained at high calcination temperature. This trapped electron was characterised by an 29-line EPR signal corresponding to unpaired electron over four equivalent vanadium. The trapped electron is responsible for reduction of Ce^{4+} into Ce^{3+} whereas V^{5+} remains intact.

$$V_2O_5 + 2\,CeO_2 \rightarrow V_2O_{5-x} \boxdot 2\,CeO_{2-y} \rightarrow 2CeVO_4 + \tfrac{1}{2}\,O_2$$

Several authors [18, 26] have confirmed by XRD, Raman and IR spectroscopy that the oxidation state in $CeVO_4$ is V^{5+} and Ce^{3+}.

In this work, when copper is present in the solid with the same atomic content as vanadium (1Cu1V10Ce), the orthovanadate phase is observed. However, no $CeVO_4$ phase is revealed for the 10Cu1V10Ce solid but a copper oxide phase is evidenced for all calcinations temperature. According to the thermal analysis results, it seems that the $CeVO_4$ formation phase was inhibited by the high copper content. To investigate the insertion of copper and vanadium ions in the CeO_2 matrix, an EPR study was performed.

EPR measurements

EPR is a powerful and sensitive technique for investigating the oxidation states, surfaces, bulk coordination and the physical form of a transition metal oxide. EPR technique has been extensively employed to study powder oxide catalytic systems, in particular Cu–Ce and V–Ce oxide [2, 3, 12, 19]. In order to study the existence of interaction effects and compare the ternary systems (Cu–V–Ce) with binary systems (Cu–Ce and V–Ce), the EPR spectra of Cu–V–Ce compounds were measured. Figure 3 shows the EPR spectra of 1Cu1V10Ce and 10Cu1V10Ce solids calcined under air at different temperatures between 400 and 600 °C. The spectra are constituted of a superposition of several signals with different g values in the range ≈2. These signals are characteristic to copper and cerium species. The EPR spectra of these components were compared with binary compounds (Cu–Ce) studied in a previous work by Aboukaïs et al. [12]. A signal with g values <2 was observed and designated as Ce. Similar signal was observed in the literature [23] and assigned to an interaction between conduction electrons and the vacant orbital of Ce^{4+} ions in the CeO_2 matrix. It is important to notice that these signals were also present on the EPR spectrum of the ceria support before the impregnation of vanadium or/and

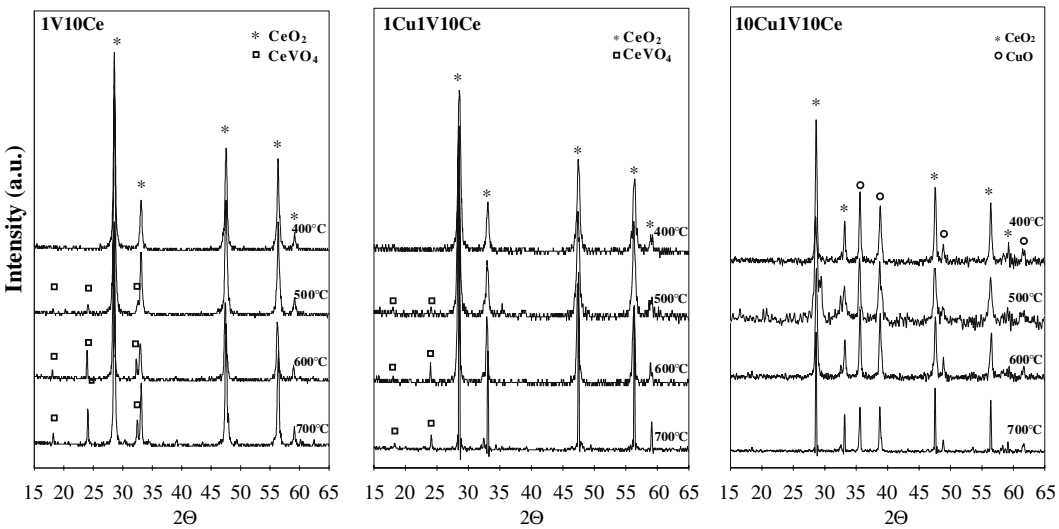

Fig. 2 X-ray diffraction patterns of 1V10Ce, 1Cu1V10Ce and 10Cu1V10Ce at different temperature treatments

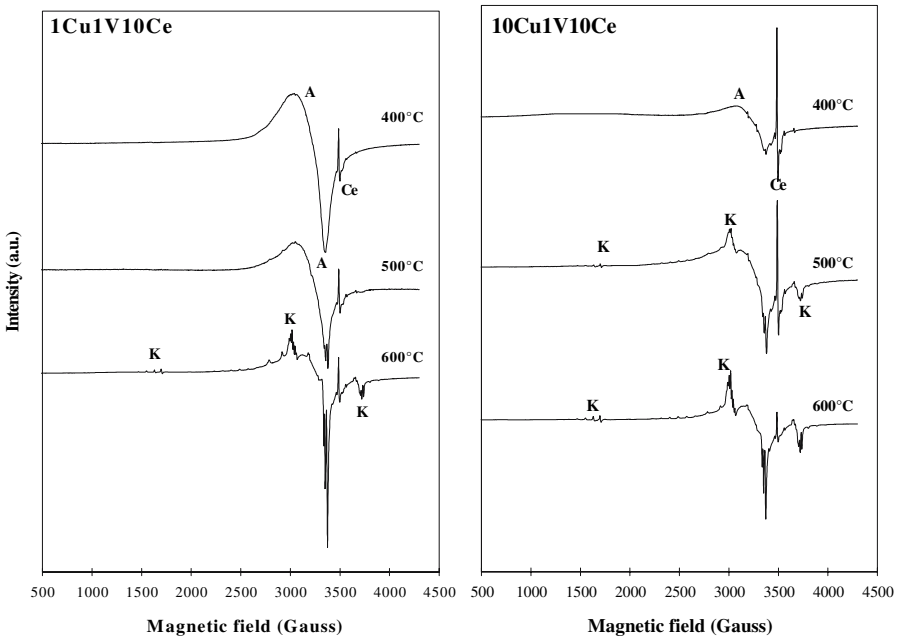

Fig. 3 Experimental EPR spectra recorded at –196 °C for 1Cu1V10Ce and 10Cu1V10Ce at different temperature treatments

copper salts. Other signals with g values >2 were attributed to Cu^{2+} species. The spectrum (Fig. 4) shows complex hyperfine structures consisting of an ''A'' signal due to isolated monomeric Cu^{2+} ions on CeO_2, and a set of ''K'' signals characteristic of Cu^{2+} dimers. Similar EPR spectra were reported in literature for Cu–Ce oxides [11, 12, 27–30] prepared by coprecipitation and impregnation methods and calcined above 700 °C.

The EPR parameters of signal ''A'' are reported in Table 2. After the calcination at 400 °C of the dried solids, all the recorded EPR spectra revealed this signal ''A'' characteristic of Cu(II) species. It is clear that the EPR parameters of the Cu(II) species were very similar for the two ternary compounds 1Cu1V10Ce and 10Cu1V10Ce, whereas for the 1Cu10Ce sample, the parameters were slightly different. These EPR parameters observed for the samples were very similar to those of Cu^{2+} signal assigned to well-dispersed Cu^{2+} ions on ceria. In all cases, the value of the splitting constant (≅130 G) indicates that the Cu(II) species are located in octahedral sites tetragonally distorted and surrounded by less than six ligands. However, for the ternary solids (1Cu1V10Ce and 10Cu1V10Ce) sample, the Δg value ($\Delta g = g_{//} - g_{\perp}$) is more higher (respectively $\Delta g = 0.318$ and 0.316) than in the case of the binary sample (1Cu10Ce, $\Delta g = 0.289$). This difference reveals that the symmetry site distortion seems to be more pronounced for ternary oxide (Cu–V–Ce). This phenomenon may result from the presence of the vanadium (V) species in the solid which could modify the environment of copper species. When the calcination temperature increases (at 600 °C), in addition to monomeric Cu^{2+} species signal, a ''K signal'' consisting of parallel and perpendicular

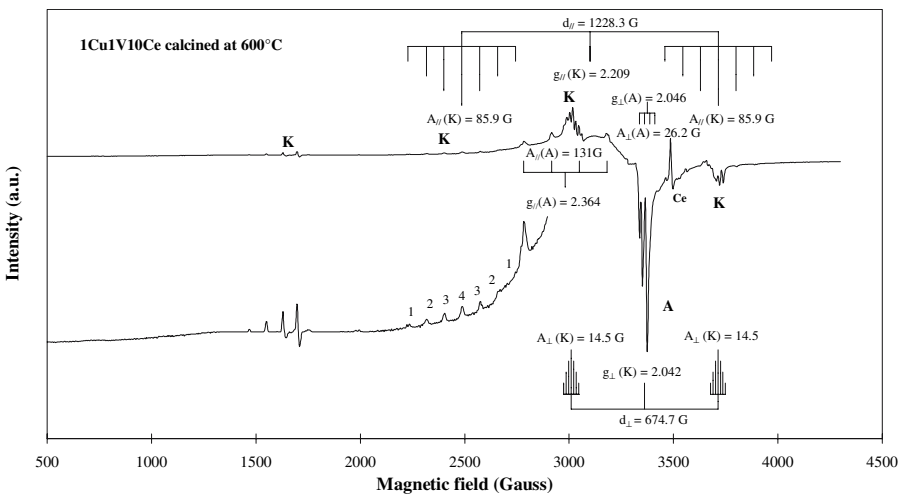

Fig. 4 Experimental EPR spectrum for 1Cu1V10Ce sample calcined at 600 °C

Table 2 EPR parameters of Cu^{2+} monomeric species (A signal) in the different samples

Sample	$g_{//}$	$g_{\perp}$	g_{iso}	Δg	$A_{//}$	$A_{\perp}$	A_{iso}
1Cu1V10Ce	2.364	2.046	2.152	0.318	131	26.2	61.1
10Cu1V10Ce	2.357	2.043	2.148	0.314	130	26	60.7
1Cu10Ce	2.321	2.032	2.128	0.289	131	27.5	62.0
CuCe [12]	2.237	2.037	2.104	0.200	160	22	68.0

($A_{//}$, $A_{\perp}$ and A_{iso} in Gauss)

hyperfine structures is evidenced (Table 3, Fig. 4). A well-resolved copper dimer signal is observed when the Cu–V–Ce oxides are calcined at 600 °C. A similar signal has been obtained in the case of CuCe oxide and has been attributed to copper(II) ion pair [12, 27]. In fact, seven components with relative intensities 1:2:3:4:3:2:1 are observed in the parallel and perpendicular components of the fine structure. Such a structure is produced by the coupling between two unpaired electrons (S = 1) with the nuclear spins of two Cu^{2+} ions (I = 3/2 + 3/2). Moreover, a well-resolved signal with a weak intensity is observed at half normal magnetic field (≅1650 G); its EPR parameters are given in Table 3. The fine structure of the spectrum and the presence of the half magnetic field signal are characteristic of copper(II) ion dimers. The EPR dimer parameters are very similar for the three samples: 1Cu10Ce, 1Cu1V10Ce and 10Cu1V10Ce and are slightly different from these obtained in literature [12, 27]. The different preparation method could explain this variation. In this work, it could be noticed that the same copper dimer species consisting of two Cu^{2+} ions bridged by oxygen are observed for all samples. Thus, the vanadium presence in the solids has no effect on the copper dimer EPR parameters. Finally, it is important to notice that no signal relative to V(IV) species is observed indicating that the totality of the vanadium species are in V(V) oxidation state. In order to characterise the vanadium species in these solids, a ^{51}V-MAS-NMR study was performed.

^{51}V-MAS-NMR measurements

Solid-state ^{51}V nuclear magnetic resonance (NMR) is a suitable technique to investigate supported V^{5+} oxides since the nuclear spin of vanadium is 7/2; its natural abundance is almost 100% and its capability to discriminate between different coordination environments of vanadium oxides [25, 31]. ^{51}V-MAS-NMR spectra of 1V10Ce solid previously calcined at different temperature between 400 and 700 °C are shown in Fig. 5. The solid calcined at 400 °C gives two well-resolved signals: the first one is characterised by an isotropic chemical shift δ_{iso} = –750 ppm and numerous associated symmetric spinning sidebands; the second one by δ_{iso} = –609 ppm with an asymmetry of the sidebands pattern. This latter signal is well known and can be typically attributed to V_2O_5 [32–34]. Note that this phase was not detected by XRD but ^{51}V-MAS-NMR possesses a higher sensitivity. The species responsible of the signal at δ_{iso} = –750 ppm has been previously observed for V–Ce–O systems [31] and corresponds to slightly distorted tetrahedral sites. In addition, a broad signal appears on this spectrum which could reveal the presence of amorphous V^{5+} species in this sample.

With the increase of the calcination temperature (500 °C), a strong decrease of the signal at δ_{iso} = –750 ppm is observed as well as a slight increase of the signal related to polycrystalline V_2O_5. It is important to notice the appearance of a new signal centrered at δ_{iso} = –427 ppm. Its intensity strongly increases after calcination treatments at higher temperature whereas other signals completely disappear. The evolution of the signal at δ_{iso} = –427 ppm can be linked to the progressive formation of $CeVO_4$ evidenced by XRD. In agreement with literature data, this signal corresponds to V^{5+} sites located at the centre of isolated tetrahedral of the orthovanadate $CeVO_4$ structure. In this solid, $CeVO_4$ seems to be result from the progressive reaction of the tetrahedral V(V) species and

Table 3 EPR parameters of Cu^{2+} dimer species (K signal) in the different samples calcined at 600 °C

Sample	$g_{//}$	$g_{\perp}$	g_{iso}	$A_{//}$	$A_{\perp}$	A_{iso}	$d_{//}$	$d_{\perp}$
1Cu1V10Ce	2.209	2.042	2.097	85.9s	14.5	38.3	1228.3	674.7
10Cu1V10Ce	2.209	2.041	2.097	86.4	14.5	38.5	1227.1	674.7
1Cu10Ce	2.209	2.042	2.097	86.4	14.4	38.4	1228.3	676.7
CuCe [12]	2.217	2.043	2.101	85.0	12.0	36.3	1264.0	693.0

($A_{//}$, $A_{\perp}$, A_{iso}, $d_{//}$ and $d_{\perp}$ in Gauss)

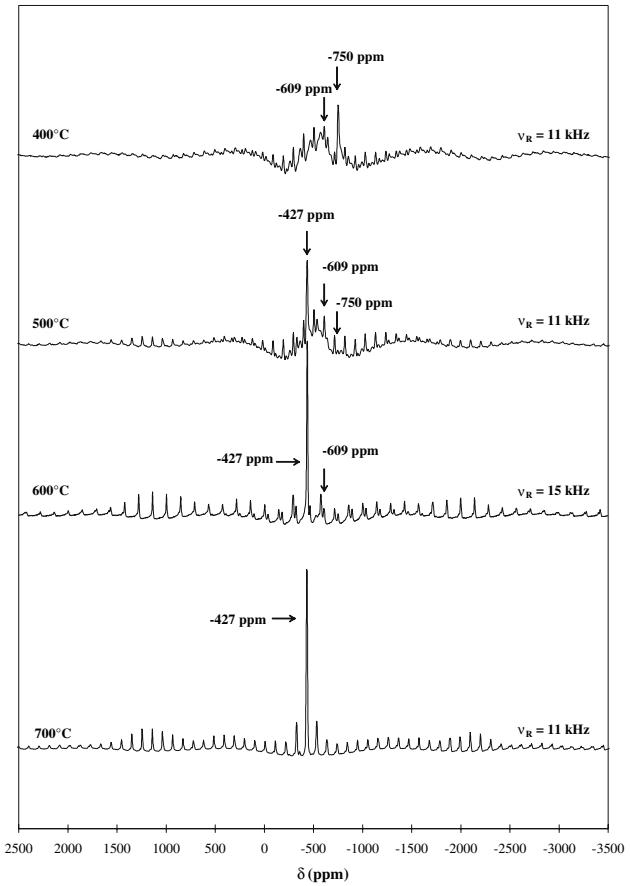

Fig. 5 ^{51}V-MAS-NMR spectra of 1V10Ce sample calcined at different temperatures

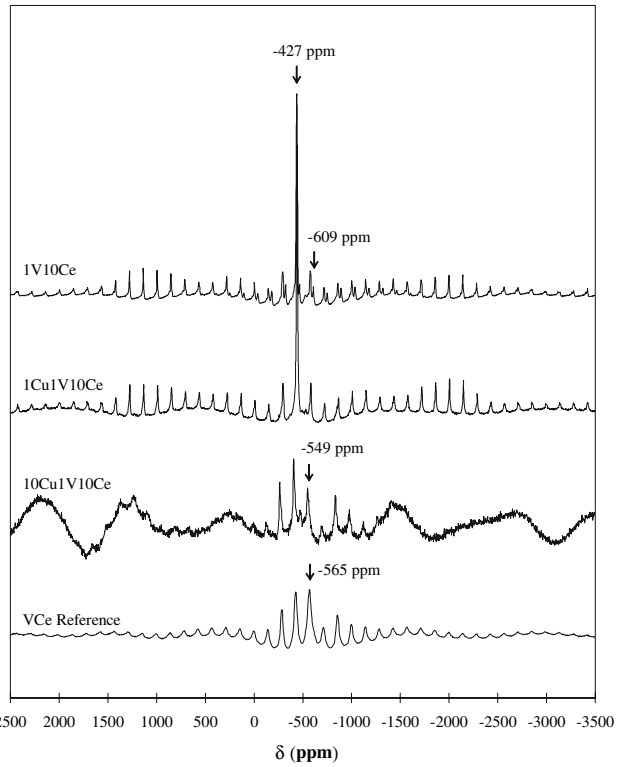

Fig. 6 ^{51}V-MAS-NMR spectra of 1V10Ce, 1Cu1V10Ce and 10Cu1V10Ce calcined at 600 °C and VCe reference compound [29]. ν_r = 15 kHz

ceria. It can be excluded that these tetrahedral species firstly agglomerate to give V_2O_5 and then react with ceria. It is in accordance with previous work [18] of Martinez-Huerta et al. which suggest that Ce^{3+}–O^{2-}–V^{5+} sites form when vanadia is well dispersed on the CeO_2 support. These Ce^{3+}–O^{2-}-V^{5+} sites can be considered precursors of a well-developed $CeVO_4$.

In order to evaluate the effect of the presence of copper in V-Cu/CeO_2 solids on the nature of vanadium species, 1Cu1V10Ce, 10Cu1V10Ce have been characterised by ^{51}V-MAS-NMR considering solids calcined at 600 °C (Fig. 6).

The spectrum of 1Cu1V10Ce solid calcined at 600 °C exhibits the signal relative to $CeVO_4$ (δ_{iso} = –427 ppm) slightly less intense than in the case of 1V10Ce solid. The signal corresponding to V_2O_5 (δ_{iso} = –609 ppm) is not detected in 1Cu1V10Ce suggesting that the presence of copper in this solid inhibits the formation of this oxide phase. With the increase of the copper content in Cu–V–Ce oxides (10Cu1V10Ce), neither $CeVO_4$ nor V_2O_5 are evidenced in the solid. In these solids treated at 600 °C, the high concentration of copper appears to have an important effect on the nature and the environment of V^{5+} sites. Indeed, our results show that the formation of V_2O_5 and the reaction leading to the formation of $CeVO_4$ are hindered.

In fact, 10Cu1V10Ce solid gives a signal characterised by δ_{iso} = –549 ppm and an asymmetry of the sideband pattern. The shape of this sideband pattern and the position of the isotropic component were found close to NMR parameters obtained for vanadium species in distorted octahedral sites (V–O–V chains) in V–Ce oxides with low vanadium content [31]. Species with the same geometrical environment could be formed in 10Cu1V10Ce but the shift of the δ_{iso} component observed in the presence of copper toward low magnetic values can be discussed in the light of the literature data [32, 35, 36].

V^{5+} species in 10Cu1V10Ce appear to be less shielded than the polymeric V–O–V in V-Ce oxides [31]. It can be assumed that the magnetic shielding of vanadium is directly affected by the electron density around oxygen atoms which depends on the electronegativity of the second neighbouring metal atom in the second coordination sphere. ^{51}V-NMR studies on different metavanadates [32, 35] and on V_2O_5–Nb_2O_5 [36] catalysts showed that the values of isotropic chemical shifts of vanadium move toward more negative values as the electronegativity of the second metal atom decreases. In our case, a shift of δ_{iso}

toward a less negative value is expected as Cu possesses a higher electronegativity value than Ce. Consequently, the shift of the δ_{iso} component in the presence of copper is due to a smaller electron density around vanadium in 10Cu1V10Ce in comparison with V-Ce oxide. This observation shows that vanadium is in interaction with copper in Cu–V–Ce oxide.

XPS measurements

The surface composition of Cu–V–Ce oxides calcined at 600 °C has been studied by X-ray photoelectron technique which confirmed the oxidation state of copper and vanadium elements in these catalysts. Qualitative and quantitative XPS analyses have been reported (Table 4) for the binary and the ternary oxides to determine and compare the bulk and surface composition. Concerning the qualitative study, the binding energies were determined by using the Ce 3d satellite peak at 916.7 eV for standardisation. In the XPS results (Table 4), binding energy of 933.5–934 eV for the Cu $2p_{3/2}$ peak, $Auger_{L3M4,5M4,5}$ peak and shake-up peaks are characteristic of Cu^{2+} species and specially of CuO [37]. These results showed that Cu^{2+} species were present at the surface on all oxide systems. The binding energy of the V 2p3/2 level for the three samples (Table 4) near to 517 eV is characteristic to the literature [38–41] values for V^{5+}. These results are in accordance with the previous XRD, EPR and NMR analysis.

Furthermore surface atomic ratios Cu/Ce and V/Ce generally possess higher value than the bulk atomic ratios (Table 4). This observation was expected since V and Cu were impregnated on calcined CeO_2 support. Additional information on the dispersion of V and Cu on the CeO_2 surface can be deduced from Cu/V surface atomic ratio. For 1Cu1V10Ce experimental n_{Cu}/n_V from XPS reaches 1.89 whereas a theoretical homogeneous dispersion of these elements corresponds to a value of 0.99. This result indicates that Cu^{2+} ions are more dispersed on the surface than V^{5+} ions. It can be suggested that the low dispersion of V^{5+} arises from the formation of $CeVO_4$ crystallites. With the increase of the copper content (10Cu1V10Ce solid), we notice a Cu/V surface atomic ratio of 6.85, lower than the theoretical homogeneous distribution of V and Cu on the CeO_2 surface. In agreement with EPR data showing the presence of Cu^{2+} species inside the CeO_2 matrix, this result tends to confirm the incorporation of copper in the solid. This phenomenon also explains on the contrary a better dispersion of vanadium on the solid surface. It is in accordance with the ^{51}V-MAS-NMR study which revealed for the 10Cu1V10Ce sample, polymeric V–O–V chains in interaction with a copper–cerium system. This phenomenon could be due to the impregnation method on the ceria support which possesses a low specific area (35 m^2/g). Indeed, after copper and vanadium impregnation on the ceria and thermal treatment at 600 °C, the specific area of the 10Cu1V10Ce solid is equal to 6 m^2/g. This value is close to those obtained for pure CuO (5 m^2/g). The high concentration of copper precursor seems to block the pores of the support. After thermal treatment at 600 °C, primarily copper (II) species are not only inserted in the CeO_2 solid but also cover the ceria surface. Besides, the vanadium species could be located on the upper layer of the solid. But these species are in interaction with a copper ceria matrix as mentioned above by the ^{51}V-MAS-NMR. In fact, vanadium and cerium species react to form $CeVO_4$ grains. This phenomenon is inhibited by the copper content because copper ions are preferentially incorporated into the ceria matrix. Thus, this could explain the absence of the $CeVO_4$ phase in 10Cu1V10Ce sample.

Conclusion

The combination of different physicochemical techniques used in this study has allowed us to define the nature and evaluate the stability of different copper and vanadium species present in Cu–V–Ce–O compounds. X-ray diffraction and thermal analysis revealed cerium orthovanadate phase formation during the calcination of the 1Cu1V10Ce solid. This $CeVO_4$ phase is not observed for the 10Cu1V10Ce sample. The ceria orthovanadate phase formation is inhibited by the presence of a high copper content in the solid. The EPR study revealed two well-resolved copper signals: the first corresponds to isolated Cu^{2+} species located in octahedral sites tetragonally distorted surrounded by less than six ligands and the second to

Table 4 Experimental XPS data and bulk atomic ratio for the different sample calcined at 600 °C

Sample	$E_{l\ Cu2p/2}$ (eV)	$Cu_{L3M4,5M4,5}$ (eV)	$E_{lV2p3/2}$ (eV)	$n_{Cu2p3/2}/n_{Ce3d}$	$n_{V2p3/2}/n_{Ce3d}$	$n_{Cu2p3/2}/n_{V2p3/2}$
1V10Ce	–	–	517.2	–	0.21 (0.101)[a]	–
1Cu10Ce	934.0	917.2	–	0.24 (0.098)[a]	–	–
1Cu1V10Ce	933.9	917.6	517.0	0.51 (0.101)[a]	0.27 (0.102)[a]*	1.89 (0.99)[a]
10Cu1V10Ce	933.5	918.0	516.7	5.62 (0.972)[a]	0.82 (0.097)[a]	6.85 (10.02)[a]

( )[a] bulk atomic ratio determined by chemical analysis from Vernaison Analysis Center

Cu^{2+} dimers consisting to two Cu^{2+} ions bridged by oxygen. The same copper species were observed in both samples (1Cu1V10Ce and 10Cu1V10Ce). The ^{51}V-MAS-NMR confirmed the presence of $CeVO_4$ phase for 1Cu1V10Ce sample and revealed polymeric V–O–V chains in interaction with a copper ceria matrix for 10Cu1V10Ce. Finally, the XPS study showed an exaltation of vanadium ions on the solid surface. Copper ions are more preferentially incorporated than vanadium atoms in ceria matrix. Thus the high copper content in the CuVCe oxides inhibits the $CeVO_4$ phase formation.

Acknowledgements The authors would like to thank L. Gengembre for assistance with the XPS analysis and B. Revel for the NMR measurements. The ''Conseil Général du Nord'', the ''Région Nord-Pas de Calais'', and the European Community (European Regional Development Fund) are gratefully acknowledged for financial supports in the purchase of the EPR and thermal analysis apparatus.

References

1. Radwan NRE, Turky AEM, El-Shobaky GA (2002) Colloids Surf A 203:205
2. Lamonier C, Bennani A, D'Huysser A, Aboukaïs A, Wrobel G (1996) J Chem Soc Faraday Trans 92:131
3. Martinez-Arias A, Cataluna R, Conesa JC, Soria J (1998) J Phys Chem B 102:809
4. Li Y, Fu Q, Flytzani-Stephanopoulos M (2000) Appl Catal B 27:179
5. Dow W, Wang Y, Huang T (2000) Appl Catal A 190:25
6. Breysse M, Guenin M, Claudel B, Latreille H, Véron J (1972) J Catal 27:275
7. Oran U, Uner D (2004) Appl Catal B 54:183
8. Nakatsuji T, Rustoistenmäki J, Komppa V, Tanaka Y, Uekusa T (2002) Appl Catal B 38:101
9. Shido T, Iwasawa Y (1992) J Catal 136:493
10. Mariño F, Descorme C, Duprez D (2004) Appl Catal B 54:59
11. Ranga Rao G, Ranjan Sahu H, Gopal Mishra B (2003) Colloids Surf A 220:261
12. Aboukaïs A, Bennani A, Lamonier-Dulongpont C, Abi Aad E, Wrobel G (1996) Colloids Surf A 115:171
13. Bera P, Aruna ST, Patil KC, Hegde MS (1999) J Catal 186:36
14. Harrison PG, Ball IK, Azelee W, Daniell W, Goldfarb D (2000) Chem Mater 12:3715
15. Grzybowska-Swierkosz B (1997) Appl Catal A 157:263
16. Ahlström AF, Odenbrand O (1990) Appl Catal 60:157
17. Lietti L, Forzatti P (1994) J Catal 147:241
18. Martinez-Huerta MV, Coronado JM, Fernandez-Garcia M, Iglesias-Juez A, Deo G, Fierro JLG, Banares MA (2004) J Catal 225:240
19. Cousin R, Dourdin M, Abi-Aad E, Courcot D, Capelle S, Guelton M, Aboukaïs A (1997) J Chem Soc Faraday Trans 93(21):3863
20. Eckert H, Wachs I (1989) J Phys Chem 93:6786
21. Mastikhin V, Terskikh V, Lapina OB, Filiminova S, Seidl M, Knozinger H (1995) J Catal 156:1
22. Courcot D, Grzybowska B, Barbaux Y, Rigole M, Ponchel A, Guelton M (1996) J Chem Soc Faraday Trans 92:1609
23. Abi-Aad E, Bechara R, Grimblot J, Aboukaïs A (1993) Chem Mater 5:793
24. Matta J, Courcot D, Abi-Aad E, Aboukaïs A (2001) J Therm Anal Calorim 66:717
25. Cousin R, Courcot D, Abi-Aad E, Capelle S, Amoureux JP, Dourdin M, Guelton M, Aboukaïs A (1999) Colloids Surf A 158:43
26. Opara Krasovec U, Orel B, Surca A, Bukovec N, Reisfeld R (1999) Solid State Ionics 118:195
27. Aboukaïs A, Bennani A, Aïssi CF, Wrobel G, Guelton M, Vedrine JC (1992) J Chem Soc Faraday Trans 88:615
28. Martinez Arias A, Fernandez Garcia M, Galvez O, Coronado JM, Anderson JA, Conesa JC, Soria J, Munuera G (2000) J Catal 195:207
29. Martini G, Basseti V, Ottaviani MF (1980) J Chim Phys 77:311
30. Soria J, Martinez-Arias A, Martinez-Chaparro A, Conesa JC, Schay Z (2000) J Catal 190:352
31. Matta J, Courcot D, Abi-Aad E, Aboukaïs A (2002) Chem Mater 14:4118
32. Lapina OB, Mastikhin VM, Shubin AA, Krasilnokov VN, Zamaraev KI (1992) Prog Nucl Magn NMR Spectrosc 24:457
33. Skibsted J, Nielsen NC, Bildsoe H, Jacobsen HJ (1992) Chem Phys Lett 188:405
34. Fernandez C, Bodart P, Amoureux J-P (1994) Solid State Nucl Magn Reson 3:79
35. Hayakawa S, Yoko T, Sakka S (1993) Bull Chem Soc Jpn 66:3393
36. Smits RHH, Seshan K, Ross JRH, Kentgens APM (1995) J Phys Chem 99:9169
37. Bechara R, Aboukaïs A, Guelton M, D'Huysser A, Grimblot J, Bonnelle JP (1990) Spectrosc Lett 23:1237
38. Cazzanelli E, Mariotto G, Passerini S, Smyrl WH, Gorenstein A (1999) Solar Energy Mater Solar Cells 56:249
39. Cornaglia LM, Lombardo EA (1995) Appl Catal A 127:125
40. Occhiuzzi M, Tutti S, Cordischi D, Dragone R, Indovina V (1996) J Chem Soc Faraday Trans 92:4337
41. Wu Q, Thissen A, Jaegermann W, Liu M (2004) Appl Surf Sci 236:473